## Membrane fusion and drug delivery with carbon nanotube porins

Nga T. Ho<sup>a,b,1</sup>, Marc Siggel<sup>c,1</sup>, Karen V. Camacho<sup>a</sup>, Ramachandra M. Bhaskara<sup>c</sup>, Jacqueline M. Hicks<sup>a,d</sup>, Yun-Chiao Yao<sup>a,b</sup>, Yuliang Zhang<sup>a</sup>, Jürgen Köfinger<sup>c</sup>, Gerhard Hummer<sup>c,e,2</sup>, and Aleksandr Noy<sup>a,b,2</sup>

<sup>a</sup> Materials Science Division, Physical and Life Sciences Directorate, Lawrence Livermore National Laboratory, Livermore, CA 94550, USA; <sup>b</sup>School of Natural Sciences, University of California Merced, Merced, CA 93434, USA; <sup>c</sup>Department of Theoretical Biophysics, Max Planck Institute of Biophysics, 60438 Frankfurt am Main, Germany; <sup>d</sup>Department of Regenerative Medicine and Cellular Therapies, University of Nottingham, Nottingham, UK; <sup>e</sup>Institute of Biophysics, Goethe University Frankfurt, 60438 Frankfurt am Main, Germany

This manuscript was compiled on April 9, 2021

11

12

10

11

15

21

23

24

25

Drug delivery mitigates toxic side effects and poor pharmacokinetics of life-saving therapeutics and enhances treatment efficacy. However, direct cytoplasmic delivery of drugs and vaccines into cells has remained out of reach. We find that liposomes studded with 0.8 nm carbon nanotube porins (CNTPs) function as efficient vehicles for direct cytoplasmic drug delivery by facilitating fusion of lipid membranes and complete mixing of the membrane material and vesicle interior content. Fusion kinetics data and coarse-grained MD simulations reveal an unusual mechanism where CNTP dimers tether the vesicles, pull the membranes into proximity, and then fuse their outer and inner leaflets. Liposomes containing CNTPs in their membranes and loaded with an anticancer drug, doxorubicin, were effective in delivering the drug to cancer cells, killing up to 90% of them. Our results open an avenue for designing efficient drug delivery carriers compatible with a wide range of therapeutics.

Carbon nanotube porins | Membrane fusion | Drug delivery | Liposomes

M odern medicine relies on an extensive arsenal of drugs to combat deadly diseases such as pneumonia, tuberculosis, HIV-AIDS, and malaria (1). Chemotherapy agents have prolonged lives for millions of cancer patients, and in some cases, cured the disease or turned it into a chronic condition (2). Yet, the safe and efficient delivery of drugs to target tissues remains a major challenge. Drugs are often poorly soluble, strongly toxic to other tissues or face rapid degradation in the different chemical environments in an organism (3). They can accumulate in non-target tissues, bind to other cellular components, or may not internalize efficiently into the target cells (4). Liposomal delivery systems aim to mitigate these problems by encapsulating drugs in external carriers that circulate through the bloodstream (5–7). However, these strategies involve a trade-off between enhancing liposomal stability on the way to the target and easing payload release into the cytosol of the target cell (5). Most current liposomal delivery strategies rely on the endosomal pathway for cell entry, which is inherently inefficient and often results in degradation of the cargo (8). Commonly used cationic lipids, which enhance liposomal fusion with the target membrane and thus enhance endosomal escape, proved to be toxic (9, 10). Another method attempting direct delivery via the plasma membrane required the placement of SNARE-like peptides on the target membrane, which severely limits clinical applications (11).

An alternative approach would facilitate direct payload delivery from liposomes through the plasma membrane into the cell interior by facilitating direct fusion of the carrier membrane with the cell. Our previous molecular dynamics (MD) simulations (12) indicated that carbon nanotube porins

(CNTPs)—short pieces of carbon nanotubes inserted into lipid membranes (13)—could potentially facilitate fusion of lipid membranes. That theoretical study raised the intriguing possibility that ten nanometer-long and 1.5 nanometer-wide CNTPs. which resemble hydrophobic stalks of influenza hemagglutinin and HIV-1 Env (14–17), can insert into opposite membranes, promote the formation of a short-lived hourglass-shaped fusion intermediate where the inner leaflets are still intact, and then drive a transition to full fusion (12). However, the simulation study left open many questions, whether CNTP mediated fusion was even practically possible, and whether the concept was applicable for drug delivery. Moreover, how additional parameters such as thickness or aggregation of CNTPs might affect the fusion kinetics in a real-world setting remains largely unclear. In this study we explore the hypothesis that small diameter CNTPs can serve as generic minimal synthetic analogs of viral fusion machines. We show that 0.8 nm diameter CNTPs indeed facilitate efficient membrane fusion. Moreover, our in vitro experiments demonstrate that CNTP-studded liposomes loaded with an anticancer drug enable efficient payload delivery into target cells. Our studies also reveal a surprising mechanism of fusion, where CNTP dimers show strong fusogenic activity.

33

35

36

37

38

39

40

41

42

43

44

47

48

49

50

51

52

## **Significance Statement**

The plasma membrane protects cell content from the outer environment. Overcoming this obstacle and delivering drugs efficiently into cells still remains a major hurdle for modern pharmacology and medicine. We developed and demonstrated a simple nanomaterial platform—a dimer of small diameter carbon nanotube porins (CNTPs)—which functions as a potent membrane fusogen. Molecular simulations revealed a distinct fusion mechanism. CNTP-studded vesicles loaded with a chemotherapeutic agent, doxorubicin, delivered the drug to cancer cells, killing a majority of them. Our work opens up new opportunities for understanding membrane fusion mechanisms, designing synthetic fusogens, and developing simple and efficient drug carriers for delivery of therapeutics and vaccines.

NH and AN designed fusion and drug delivery studies. NH performed the fusion assays. NH, KC, JH, and JY performed drug delivery studies, NH, KC, and YZ analyzed the data. MS, RMB, JK, and GH designed computer simulations. MS performed simulations and analyzed data with help from RMB, JK, and GH. AN, GH, and JK directed the work. MS, NTH, GH and AN wrote the manuscript. All authors participated in revising and editing the final draft.

Some of the results reported here have been disclosed as a part of a provisional patent filing

<sup>&</sup>lt;sup>1</sup> N.H.contributed equally to this work with M.S.

 $<sup>^2\</sup>mbox{To}$  whom correspondence should be addressed. E-mail: gerhard.hummer@biophys.mpg.de, noy1@llnl.gov

## Results and Discussion

56

57

58

59

60

61

62

63

64 65

66

67

68

71

72

73

74

77

78

79

80

81

82

83

84

85

86

87

88

89

90

91

92

93

94

97

98

99

100

101

102

103

104

105

106

107

108

109

110

111

112

114

**CNTPs-mediated vesicle fusion.** We first tested our hypothesis that CNTPs can promote vesicle fusion by adopting a widely used de-quenching lipid mixing assay (18). We mixed large unilamellar 1,2-dioleoyl-sn-glycero-3-phosphocholine (DOPC) vesicles containing 0.8 nm CNTPs in the lipid bilayer (CNTP-LUVs) with another population of pure DOPC vesicles containing lipids labeled with an NBD dye (NBD-LUVs) at a concentration just above the self-quenching threshold (19). As the lipids from different vesicles mixed during fusion, the NBD dye de-quenched (Fig. 1A,B), allowing us to quantify this process by monitoring the change in the dye fluorescence. Indeed, after mixing of these two vesicle populations the fluorescence signal rose on the timescale of tens of minutes before eventually plateauing. By contrast, fluorescence kinetics recorded in control experiments where CNTP-LUVs were replaced by pure DOPC vesicles (LUVs) did not show de-quenching (Fig. 1B, inset), indicating that the presence of CNTPs in the vesicle shell was critical to inducing fusion. As the CNTP concentration in vesicles increased, the de-quenching signal reached the plateau faster (Fig. 1B), again indicating that CNTPs were responsible for the fusion events. Surprisingly, the fusion rate, calculated as  $2/\tau$ , with  $\tau$  the fusion half-time (see Methods for details), did not scale linearly with the CNTP concentration. Instead, it followed an inverse quadratic dependence (Fig. 1D), suggesting that the key fusion step was mediated by a CNTP dimer, formed by CNTPs associating in the membrane. Docking leveled experiments, designed to separate vesicle docking kinetics from the fusion kinetics (20), indicate that docking kinetics may also contribute to the overall kinetics at higher CNTP concentrations (see SI Appendix, Fig. S1).

To verify that our system proceeded to full fusion and complete mixing of the vesicular compartments, we set up a different dye de-quenching assay, in which the target DOPC vesicles were filled with a solution of sulforhodamin B (SRB) dye in a concentration above its self-quenching threshold. After these vesicles were mixed with the CNTP-LUVs, we observed gradual de-quenching of the SRB dye fluorescence (Fig. 1E, see also SI Appendix, Fig. S2), indicating full vesicle content mixing. Content mixing kinetics proceeded in a CNTP concentration-dependent manner and followed the same inverse quadratic dependence observed in the membrane mixing assay (Fig. 1E, inset). We also confirmed vesicle fusion, full content mixing, and the absence of content leakage in similar CNTP-mediated experiments with smaller, 100 nm diameter DOPC vesicles with 30% cholesterol (SI Appendix, Fig. S3).

As a function of temperature, the fusion rate followed an Arrhenius dependence (Fig. 1C, inset) with an activation energy,  $E_a$ , of ca. 25 kJ/mol or 10  $k_BT$  (Fig. 1C). This value is significantly smaller than the activation energy of 30  $k_BT$  that was recently reported for the spontaneous fusion of small vesicles (21), indicating that CNTPs indeed lower the energy barrier for membrane fusion. Interestingly, the activation energy showed a weak dependence on pH (Fig. 1C) with the barrier dropping by an additional 2  $k_BT$  at pH values between 4 and 5, and recovering back to the original value of 10  $k_BT$  at pH values below 4. DOPC remains in a zwitterionic charge state over the whole range of pH used in our measurements. Therefore, we believe that this behavior must originate in the charge state of the CNTP ends, which start to become protonated (22) at pH 4-5. We, therefore,

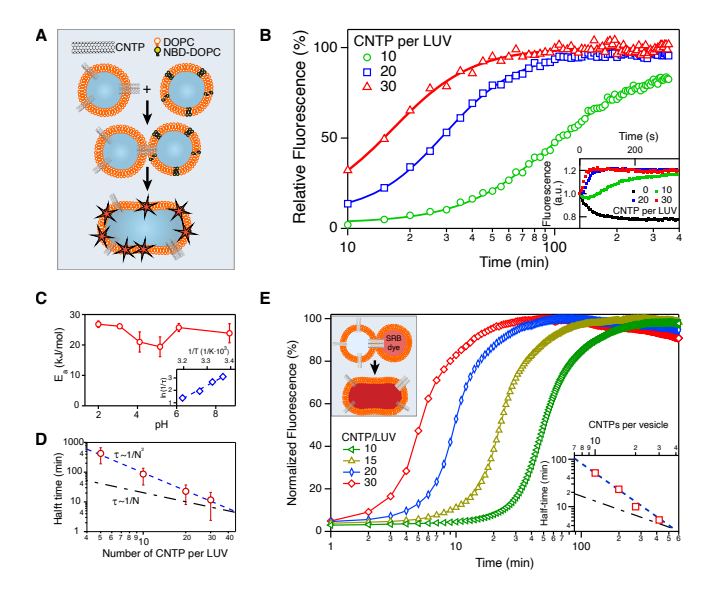


Fig. 1. CNTPs facilitate membrane fusion. (A) Schematics of the vesicle fusion assay. CNTP-LUVs fuse with the vesicles containing DOPC lipid labeled with NBD dye in self-quenching concentration, de-quench the dye, and increase its fluorescence signal. (B) Kinetics of the vesicle fusion recorded as NBD-LUVs were mixed with CNTP-LUVs with different average numbers of CNTPs per vesicle (as indicated on the graph). Solid lines represent best fits to the Hill equation. (C) Activation energy,  $E_a$  for vesicle fusion plotted as a function of pH. The inset shows a representative Arrhenius plot used to obtain the  $E_a$  values. (n=3). (**D**) Plot of the fusion half time as a function of the average number of CNTPs per vesicle (n=3 for 10, 20, and 30 CNTP/LUV and n=2 for 5 CNTP/LUV). The blue dashed line represents a fit to the second order kinetics. The dash-dotted black line, which corresponds to the first order kinetics, is provided as a guide to the eye. (E) Content-mixing assay showing fluorescence signal kinetics recorded as CNTP-LUVs were exposed to LUVs encapsulating SRB dye (each curve is an average of two runs, see SI Appendix, Fig. S2 for raw traces). An inset shows the plot of the fusion half time as a function of the average number of CNTPs per vesicle.

speculate that COOH/COO<sup>-</sup> interactions stabilize the CNTP dimers that facilitate fusion. This finding indicates that end group functionalization may be exploited to further tune the selectivity and efficiency of CNTP-mediated fusion.

Molecular dynamics simulations of vesicle fusion. We confirmed the enhanced fusogenic properties of CNTP dimers and elucidated the underlying fusion mechanism using coarse-grained MD simulations. The simulation systems contained two 15 nm DOPC vesicles with a bridging CNTP monomer, dimer, or trimer of 0.8 nm diameter inserted in their membranes (Fig. 2A, SI Appendix, Fig. S4, movie S1, SI Appendix, Table 1). To control the driving force and kinetic rate of vesicle fusion, we varied the asymmetry in the number of lipids in the outer and inner leaflets of the two vesicles, defined as  $\Delta N = N_{\rm lipids-outer} - N_{\rm lipids-inner}.$  By increasing the number asymmetry, we lowered the bilayer strain and fusion propensity of vesicles, allowing us to differentiate more clearly between the fusogenic characteristics of CNTP monomers, dimers, and trimers.

Surprisingly, CNTP dimers rapidly fused vesicles without any significant changes in fusion time over the full range of tested asymmetries. By contrast, CNTP monomers and trimers fused only vesicles with low number asymmetry, i.e., only in the presence of significant bilayer strain (Fig. 2B). At

115

116

117

118

119

120

121

122

123

124

125

126

127

128

129

131

132

133

134

135

136

high number asymmetry, monomer and trimer fusion, but not dimer fusion, slowed down dramatically, with only a few fusion events observed during the simulation time.

139

140

141

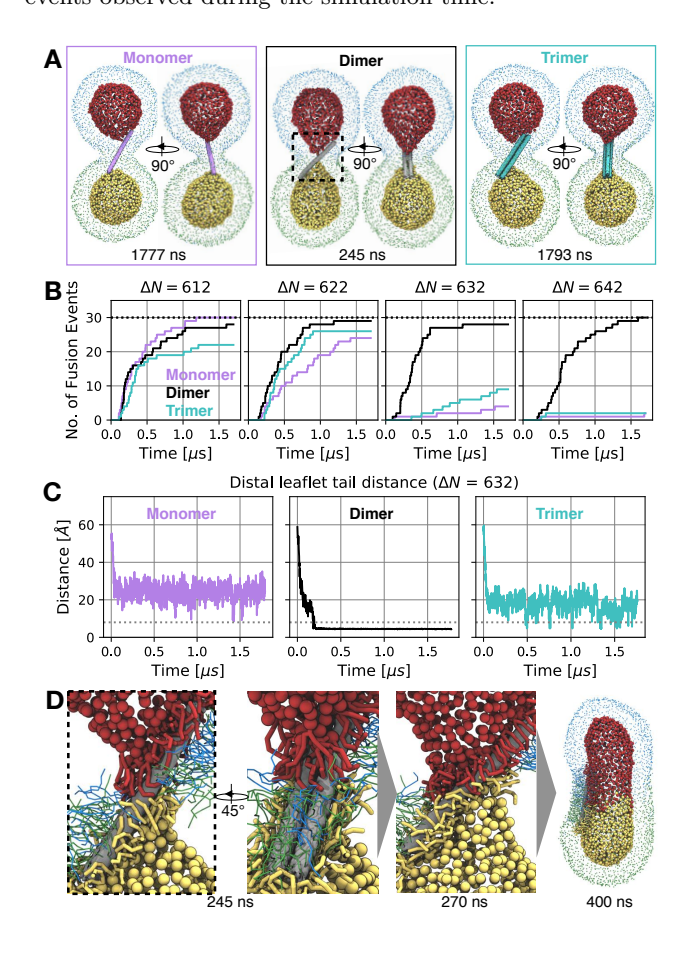


Fig. 2. Coarse-grained MD simulations of CNTP-mediated vesicle fusion. (A) Snapshots of simulated systems of a CNTP monomer (magenta), dimer (gray) and trimer (cyan) ( $\Delta N = 632$ ). Lipid phosphate groups are colored uniquely for each leaflet and vesicle (outer leaflets: blue/green for top/bottom vesicle; inner leaflets: red/yellow for top/bottom vesicle). Inner leaflet phosphate groups are drawn larger for clarity. Times of snapshots are indicated (see also movie S1). (B) Cumulative number of CNTPmediated vesicle fusion events as a function of time at different number asymmetries  $\Delta N$ . Monomer (magenta), dimer (black), and trimer (cyan) simulations are compared. A total of 30 simulations were performed for each starting configuration (indicated as black dashed line). Simulations were 1.7  $\mu$ s long. (C) Minimal distance of C5A/B tail beads of the opposing inner leaflet lipids at  $\Delta N=632$ . Exemplary trace shown for monomer, dimer, and trimer respectively. All traces for all systems are shown in SI Appendix, Fig. S6. The dashed line at 8 Å indicates contact of the opposing leaflets. (D) Zoom-in on CNTP dimer mediated fusion. Time points of snapshots are indicated. Lipids within 8 Å of the CNTP are shown. Color scheme as in (A). Inner leaflet lipids are drawn thicker for clarity. Outer leaflet phosphate groups are omitted for clarity (see also Movie S2)

We gained a more detailed insight into the fusion mechanism by monitoring the minimal distance between any two lipid tail groups in the inner leaflets of the two vesicles. In all simulations, CNTP dimers achieved initial inner-leaflet contact, which is a prerequisite for fusion, more rapidly than CNTP monomers (Fig. 2C, SI Appendix, Fig. S6). Consistently, in all relaxed pre-fusion systems, CNTP dimers distorted inner leaflets to a higher degree than monomers and trimers, leading to rapid inner leaflet contact and subsequent fusion (Fig. 2C, SI Appendix, Fig. S6, movie S1).

The asymmetric shape of the CNTP dimer explains its distinct fusogenic properties. The energetic drive to cover the hydrophobic surface of the wide faces by lipid tails (Fig. 2D, Movie S2) pulls the two vesicles together and causes significant distortion of the distal leaflets. The narrow edges of the CNTP dimer facilitate tail-tail contacts between the opposing inner leaflets. By contrast, single thin CNTPs are not coated as densely with lipid tails and consequently do not distort the distal leaflets significantly (Fig. 2A,C, SI Appendix, Fig. S6), impeding fusion. Trimers are too thick to establish sufficient tail-tail interactions (Fig. 2A,C, SI Appendix, Fig. S6), and thus fail to induce fusion on the MD simulations timescale. We emphasize that this mechanism, where the distinct geometry of the hydrophobic CNTP dimer surface facilitates lipid migration and subsequent fusion, is distinct from the common viral fusion mechanism, which relies on structural rearrangements of the fusion peptide stalks to bring the interacting membranes together (14–17). Our results may also point to the simplest structure of a membrane fusogen.

151

152

153

154

155

156

157

158

159

160

161

162

163

164

165

166

167

169

170

171

172

173

174

175

176

177

178

179

180

181

183

184

185

186

187

190

191

192

193

194

195

196

197

198

199

200

201

204

205

206

207

Our simulations also probed whether such dimer-based fusion mechanism is unique to the 0.8 nm CNTPs by testing the performance of CNTP monomers and dimers with larger diameters of 1.2 and 1.5 nm. We found that at larger diameters, the difference in fusion performance between the dimers and monomers vanished (SI Appendix Figs. S7-S11) and monomers could also catalyze fusion. This is not surprising, as CNTP monomers with a larger diameter provide sufficient hydrophobic surface to pull the lipid tails from the opposite bilayers into proximity. Conversely, the diameter is still small enough to allow contact between tails of the inner leaflets. Our previous simulations of fusion with CNTPs of 1.5 nm diameter already showed that they could catalyze membrane fusion (12). Even though CNTP dimers with larger diameters also catalyzed fusion, they did not further increase the already fast fusion rates. However, we cannot rule out that the differential dimer effect might reemerge for the larger diameter vesicles where the bilayer stress is significantly reduced, such as those typically used in the experiments. These findings align with our mechanistic model and show that the key structural features of a fusogen can be realized in multiple ways. We also note that only the dimer-based fusion mechanism is relevant for our experiments, which used a tight diameter distribution of the CNTPs  $(0.81 \pm 0.14 \text{ nm})$  (23).

We observed that not all CNTP fusion simulations proceeded directly to fusion pore formation. In several replicas across parameter sets, we noticed the formation of an intermediate with a 25 Å minimum headgroup distance (SI Appendix, Fig. S12). Visual inspection revealed a hemifusion diaphragm, where the lipids of the inner leaflets form a bilayer-like structure (SI Appendix Fig. S12, top), which was in some instances stable for long times. In this intermediate state that followed the stalk state, the outer leaflet lipids could equilibrate, while the vesicle content remained separated. The hemifusion diaphragm spontaneously opened in a distinct step, typically away from the CNTP, forming a fusion pore that completed the fusion process. The formation of hemifusion diaphragms was particularly pronounced in systems with low asymmetry (i.e., higher lipid density), where the diaphragm accommodated excess lipids of the inner leaflet. In systems with larger diameters, i.e., 1.2 and 1.5 nm, where fusion was observed over

143

145

146

147

148

150

the full range of asymmetries, high asymmetry systems fused faster because the formation of hemifusion diaphragms was disfavored.

212

213

214

215

216

217

218

220

221

222

223

224

227

228

229

230

231

232

234

235

236

237

238

239

242

243

244

245

246

247

250

251

252

253

254

255

257

258

259

260

261

262

263

264

265

266

267

268

272

Drug delivery with carbon nanotube porins. To demonstrate drug delivery to cancer cells using CNTP-mediated membrane fusion (Fig. 3A), we encapsulated a widely-used first line of defense chemotherapeutic agent, doxorubicin (DOX), in CNTP-LUVs. Systemic administration of DOX is complicated by its significant cardiac toxicity, which is often mitigated by encapsulating high amounts of the drug into PEGylated liposomal carriers (used widely in cancer treatment in commercial formulation as Doxil or Caelyx) (24). Doxil liposomes have a very slow background DOX release profile (25) that protects healthy tissues during circulation and allows the carriers to accumulate in tumors passively and then enter the tumor cells via endocytosis (26). Replacing endocytosis with a more direct fusion-based entry pathway could significantly improve the delivery efficiency for the liposome-encapsulated drugs.

To evaluate this hypothesis, we tested DOX-CNTP-LUV performance in a series of cell viability assays on two different cell lines: NG108-15 (mouse neuroblastoma and rat glioma hybrid cells) and MDA MB-231 (human breast cancer cells) (Fig. 3). For these experiments we loaded CNTP-LUVs with a relatively low encapsulated DOX concentration of 10  $\mu$ g/ml. DOX molecule size is larger than the CNTP pore size, excluding the possibility that DOX would leak through the nanotubes. Control experiments (SI Appendix, Fig. S13) also confirm the absence of long-term drug leakage from CNTP-LUVs. To mimic some of the current liposomal delivery strategies, we used smaller, 100 nm diameter liposomes with lipid composition of 70% DOPC and 30% of cholesterol. This vesicle composition also showed high fusion efficiency with an average  $\tau$  of less than 1 hour, similar to what we observed for the pure DOPC vesicles at a similar size (SI Appendix, Fig. S3A, S3B). indicating the cholesterol presence did not interfere with the fusion mechanism.

After 48 hours exposure to DOX-loaded CNTP-LUVs, cell viability decreased significantly compared to the PBS control, with only 9% of NG108 cells and 16% of MDA cells surviving the treatment (Figs. 3B, 3D(iv), 3E(iv)). The efficiency of the CNTP-LUVs loaded with 10  $\mu$ g/ml of DOX (Figs. 3B, 3C, 3D(v), 3E(v)) was mostly comparable to administering 20  $\mu$ g/ml of free DOX (Figs. 3B,C, D(v), E(v)). This observation is significant because DOX-CNTP-LUVs used in our experiments contain a much smaller overall amount of drug (10  $\mu$ g/ml) compared to what is used in commercial Doxil formulation (2 mg/ml) (27). Thus, CNTP-LUV carriers could potentially exhibit dramatically lower systemic toxicity and still would maintain the high efficiency of drug release.

By contrast, control experiments (Figs. 3B, 3D(i,ii,iii) and 3E(i,ii,iii)) with cells exposed to CNTP-LUVs and free CNTPs showed very low cytotoxicity, with typically over 85% of the cells remaining alive after the same 48 hours of exposure. These viability numbers were on par with those measured after exposure to pure PBS buffer (88% and 94% for NG108 and MDA cells, respectively). Interestingly, when pure LUVs were loaded with 20  $\mu$ g/ml of DOX, their cytotoxicity was also on par with control experiments (Figs. 3B, 3D(i), 3E(i)), showing little to no efficiency without the presence of a viable delivery mechanism.

Cell proliferation (MTT) assays results (Fig. 3C) tracked

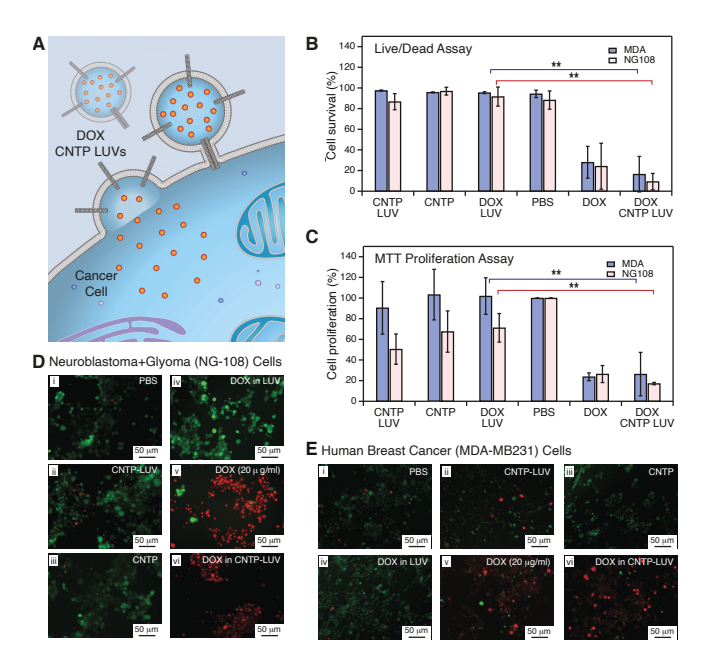


Fig. 3. Doxorubicin (DOX) delivery with CNTPs. (A) Schematic showing CNTP-LUV loaded with the DOX payload fusing to a cancer cell and delivering DOX to the cell interior. (B) Cell survival in live/dead assay after 48-hr exposure of neuroblastoma-glyoma (NG-108) and human breast cancer (MDA) cell cultures to DOX-CNTP-LUVs, CNTP-LUVs, free CNTPs, DOX-LUVs, free DOX, and PBS buffer. (N=9). (C) Results of MTT cell proliferation assay after 48-hr exposure of neuroblastoma-glyoma (NG-108) and human breast cancer (MDA) cell cultures to DOX-CNTP-LUVs, CNTP-LUVs, free CNTPs, DOX-LUVs, free DOX, and PBS buffer. (NG-108 cells: N=9; MDA cells: N=15). (**D**) Fluorescence microscopy images of NG108 cell culture with live and dead cells stained with green and red dye, respectively. Prior to imaging the cells were exposed for 48 hrs to (i) PBS buffer; (ii) CNTP-LUVs without the drug payload; (iii) CNTP solution; (iv) LUVs encapsulating DOX; (v) 20  $\mu$ g/ml of DOX; (vi) CNTP-LUVs with encapsulated DOX. (E) Fluorescence microscopy images of MDA cell culture with live and dead cells stained with green and red dye, respectively. Prior to imaging the cells were exposed for 48 hrs to (i) PBS buffer; (ii) CNTP-LUVs without the drug payload; (iii) CNTP solution; (iv) LUVs encapsulating DOX; (v) 20  $\mu$ g/ml of DOX; (vi) CNTP-LUVs with encapsulated DOX.

the trends obtained in the cell viability (live/dead) assay across all samples that we tested. Exposure of both cell lines to DOX-loaded CNTP-LUVs led to a significant decrease in the cells' proliferation ability. Control experiments where we exposed cells to CNTPs and CNTP-LUVs in the presence of free DOX in solution did not show a statistically significant cell viability decrease (SI Appendix, Figs. S14, S15), indicating that CNTP-mediated fusion was indeed the main pathway for the drug entry into the cancer cells, and that the drug did not enter through defects on the cell membranes created by free CNTPs or CNTP-LUVs. Additional experiments (SIAppendix, Fig. S16) also showed a dose-dependent cell response to CNTP-DOX-LUV treatment with higher doses resulting in progressively lower cell survival probabilities. Additional corroboration of the proposed delivery mechanism comes from experiments in which we exposed MDA cells to CNTP-LUVs loaded with a self-quenched concentration of SRB dye and observed gradual dequenching of the dye as it entered the cells (SI Appendix, Fig. S17).

We also noticed that NG108 cells exposed to free CNTPs and CNTP-LUVs showed a small decrease in the cell prolif-

273

274

275

276

277

278

279

280

281

282

283

284

286

287

288

289

290

291

eration percentage relative to the PBS buffer control. Visual observations of the NG108 cell morphology in the images of those samples showed that cells in the cultures exposed to CNTP and CNTP-LUV were still alive and building neural networks (SI Appendix, Fig. S18). Literature reports show that neural cell hybrids, such as NG108, can differentiate under certain stresses (28). Similar to the images of differentiated NG108 cells in the literature, our cultures started to form abundant neurites and varicosities after incubating them with free CNTPs and CNTP-LUVs. By contrast, the control populations of cells exposed only to the PBS buffer looked more flat and circular and had significantly fewer neurite formations (SI Appendix, Fig. S18). Thus, we hypothesize that the cells incubated with CNTP-containing samples started to differentiate instead of growing.

Conclusions and Outlook. Our results establish CNTPs as potent fusogens that exploit the unique structure and geometry of CNTP dimers to facilitate membrane fusion. Our molecular dynamics simulations revealed the mechanism of CNTP-mediated fusion and explain the observed fusion kinetics: CNTP dimers pull the membranes together with their flat faces and bring the inner leaflets into contact across their narrow faces. Researchers can apply the same principles that enable CNTP-mediated membrane fusion to design other synthetic fusogens for even more efficient and targeted delivery to specific cell types. Computational screening by molecular simulations could be used to guide the systematic design of novel nanomaterial-based fusogens and to improve the properties of the accompanying liposomes.

Our experiments demonstrate that CNTP-studded liposomes can provide the basis for constructing the long desired, but so far elusive, inert versatile carrier for direct and highly efficient delivery of drugs and DNA and RNA vaccines (29) across the plasma membrane. This strategy could bypass the endocytotic pathway entirely and thus avoid some of the problems encountered by the previous delivery strategies.

Finally, the use of carbon nanomaterials for drug delivery raises some understandable safety concerns. We note, however, that recent studies of the in vivo biocompatibility of short small diameter CNTs reported their efficient renal clearance in mice (30, 31) and nonhuman primates (32), pointing to the feasibility of using this material for therapeutics development. Further research on the long-term fate and clearance mechanisms of ultrashort carbon nanotubes in the tissues should clarify these important questions.

## **Materials and Methods**

Materials and Equipment. All the lipids (1,2-dioleoyl-sn-glycero-3phosphocholine (DOPC), 1-oleoyl-2-6-[(7-nitro-2-1,3-benzoxadiazol-4-yl)amino|hexanoyl-sn-glycero-3-phosphocholine (NBD-PC), and cholesterol) were obtained from Avanti. All the other chemicals were purchased from Sigma-Aldrich and used as received, unless specified. Live/Dead assay and MTT cellular assay kits were obtained from Abcam. The size exclusion columns for LUV separation used Sepharose CL-6B (Sigma Aldrich). The ultra short carbon nanotube porins were synthesized by sonication-assisted cutting of 0.8 nm SWCNT according to the previously published procedure (33). Previous studies have confirmed that this procedure produces CNTPs with an extremely tight diameter distribution of  $0.81\pm0.14$  nm as measured by TEM (23). Some CNTP batches were chemically coupled to the 6-amino fluorescein (6-AF) dye using an 1-Ethyl-3-(3-dimethylaminopropyl)carbodiimide (EDC) coupling procedure based on a published protocol(34). All fluorescence and absorbance

spectra was measured with the Spectramax iD3 Microplate Reader (Molecular Devices) and Cytation 5 (Biotek). Vesicle size was measured using a dynamic light scattering (DLS) setup (Malvern Analytical).

Large Unilamellar Vesicles formation. The LUVs and CNTP-LUVs were formed and characterized using previously described protocols (33). Briefly, the CNTPs were added to the lipid mixtures prior to rehydration and extrusion. The average number of CNTPs per vesicle was quantified using assays described in the same protocol (33). We note that this procedure is based on a calibrated proton permeability of an individual CNTP and thus could introduce a small systematic error. LUV and CNTP-LUVs loaded with DOX were prepared using the same protocol, but the sonication time was extended to 10 min from 2 min. To form NBD-LUVs we used 85% of DOPC and 15% of NBD-DOPC, for SRB-LUVs we added 28 mM sulforhodamine B (SRB) to the solution before sonication. All LUVs went through 10 freeze-thaw cycles to remove multilamellar vesicles. LUVs used for drug delivery experiments followed the same protocol, except that the lipid composition was 70% DOPC and 30% cholesterol, 300 mM solution of ammonium sulfate was used instead of buffered KCl solution, and the vesicles were extruded through a 100 nm membrane filter. In the final step the vesicles were purified on a column conditioned with phosphate-buffered saline (PBS) at pH 7.4. The size of LUVs were determined using DLS. The drug encapsulation efficiency was 10%, as determined by literature protocols (35). To quantify DOX leakage from DOX-loaded LUVs and CNTP-LUVs we monitored fluorescence (480ex/590em) for 18 hours at 37°C, SI Appendix, Fig. S13.

Lipid mixing and content mixing assays. To obtain a self-quenched concentration of NBD dye in LUVs we used 15% NBD-PC and 85% DOPC mixture, as determined from calibration experiments. Lipid fusion assays were performed at different pH (2, 3.15, 4.11, 5.15, 6.11, and 8.7) with buffer pH adjusted with 1 M HCl. In each fusion assay CNTP-LUVs and NBD-LUVs were mixed at 1:1 volume ratio and the fluorescence kinetics (474ex/530em) was recorded for at least 3 hours at a preset temperature maintained by the plate reader. Each assay was repeated at least 3 times. For content mixing assays, CNTP-LUVs were mixed with SRB-LUVs at 1:1 ratio in the presence of tetramethylrhodamine polyclonal antibody from Thermo Fisher to quench the signal from any leaked SRB dye. The amount of antibody used was calculated to quench at least 80% of all SRB dye contained in the sample LUV. The fluorescence kinetics (550ex/595em) was monitored for at least 18 hours at 24°C. All content fusion assays were repeated at least 2 times.

To extract fusion half-times from the fusion kinetics data we fitted the fluorescence traces to the Hill-like equation (36):

$$F = (1 + (\tau/t)^n)^{-1}$$
 [1]

where F is normalized fluorescence signal;  $\tau$  is the fusion half time; t is the time; and n is Hill coefficient. The fusion rate was then calculated as  $2/\tau$ . The values of the fit parameter n typically varied between 2 and 3.

Doxorubicin delivery to NG108-15 and MDA-MB231 cells. NG108-15 (mouse neuroblastoma x rat glioma hybrid) and MDA-MB231 cell lines were obtained from ATCC. The NG108 cells were cultured in growth media (Dulbecco's Modified Eagle Medium 1% Penicillin-Streptomycin and Hypoxanthine-Aminopterin-Thymidine 1X with 10% fetal bovine serum from Gibco) at  $37^{\circ}\mathrm{C}$  5% CO2. The MDA-MB-231 cells were cultured in DMEM/F-12, GlutaMAX $^{\mathrm{TM}}$  supplement (Thermo Fisher) with 10% fetal bovine serum from Gibco) at  $37^{\circ}\mathrm{C}$  5% CO2. The cells were seeded in 96-well plate at 5000 cells/well and cultured for 2 days before experiment. Each well was treated with growth media and sample at 1:1 volume ratio for 48 hours. Drug delivery experiments were conducted using different batches of cells purchased and cultured at different times and the results were averaged between batches wherever possible.

Cell viability quantification using live/dead assay. The live/dead dye was diluted in PBS to a final concentration of 5X (5  $\mu$ l in 1 ml of PBS). After exposure to the samples, the media was aspirated from the well and replaced by 100  $\mu$ l of dye solution. The cells were incubated for 15 minutes. The fluorescent images of cells were

recorded using a Leica fluorescence microscope with FITC (494/151 nm) and RHO (528/617 nm) filters to visualize live and dead cells respectively. The number of live and dead cells was counted using ImageJ and normalized to the total number of counted cells. The experiment was repeated 3 times, 3 wells each time, using at least 3 images per well. Since the distribution of our samples averages were not normally distributed and the samples size was less 50, we used Wilcoxon statistical analysis to test for significant differences. For some of the experiments quantifying cell response to free CNTPs, CNTPs were modified by covalent coupling of a 6-aminofluorescein (6-AF) dye to the end of the CNTP (see Materials subsection for details). Control experiments indicated that even though this modification produced slower fusion, modified and unmodified CNTPs produced similar outcomes in the fusion experiments at the 1-2 hr timescale (SI Appendix, Fig. S3C), which is still much shorter than the 48 hour time scale of the cell viability experiments.

Cell proliferation quantification using MTT assay. The media with samples were removed from wells and 50  $\mu$ l of MTT reagent and 50  $\mu$ l of PBS was added to each well. The cells were incubated at 37°C for 3 hours. After the incubation, 150  $\mu$ l of MTT solvent was added into the well. The plate was incubated overnight at room temperature in a dark box. We recorded the absorbance at 590 nm and used it (after subtracting background from PBS and MTT reagent controls) to determine the number of cells in each sample using a calibration curve established separately for each cell line. The cell proliferation percentage was normalized using PBS-exposed sample as a 100% reference.

Monitoring liposome content fusion with live cells.. MDA-MB231 cells were seeded at 10<sup>4</sup> cells per well in a 96-well plate and cultured for 48 hours. Right before the measurement, the growth media was removed from the cells and replaced with 1:1 mixture of cell media and solution of CNTP-SRB-LUVs (20 CNTP/LUV). The fluorescent signal (555ex/595em) was monitored in a plate reader.

Coarse-grained molecular dynamics simulations. All molecular dynamics simulations were setup and run as previously described (12) using the MARTINI (v. 2.2) coarse-grained model (37). Simulations were performed using GROMACS 2018.7 (38) with the recommended new parameter set for MARTINI simulations (39). The Verlet neighbor search algorithm was used to update the neighbor list, with the length and update frequency being automatically determined (nstlist = 25, rlist = 1.259). Lennard-Jones and Coulomb forces were cutoff at 1.1 nm with the potential shifted to 0 using the Verlet-shift potential modifier. Pressure was maintained at 1 bar using the Parrinello-Rahman barostat and temperature was maintained at 300 K using the velocity rescaling algorithm with characteristic coupling times of 12 and 1 ps, respectively (40, 41),

CNTPs with 0.8/1.2/1.5 nm diameter consisted of 30 rings with 5/8/10 beads each, respectively. The total length of all three types of CNTPs was 11.8 nm. For thin 0.8 nm nanotubes the force constant of improper dihedrals, which maintains stiffness, was increased to  $550 \text{ kJ} \text{ mol}^{-1} \text{ rad}^{-2}$ , whereas the 1.2 and 1.5 nm used the default values (12, 42). System starting configurations were set up following the protocol for system A of Ref. (12), where two 15 nm DOPC vesicles were stapled by a thin CNT monomer, dimer and trimer, respectively (see SI Appendix, Fig. S4). The number asymmetry was varied by removing lipids from the inner leaflets of both vesicles, respectively. All simulated systems are summarized in SI Appendix, Table 1. For each setup, 30 replicates were run with different initial velocities.

**ACKNOWLEDGMENTS.** We thank Drs. V. Frolov, A. Shnyrova, and R. Tunuguntla for help with the initial stages of this work, P. Lastrico for designing figure 3A, and anonymous reviewers for suggesting a number of additional experiments, including the docking leveled approach for evaluating fusion kinetics. AN and KC work on CNTP synthesis and vesicle fusion was supported by the U.S. Department of Energy, Office of Basic Energy Sciences, Division of Materials Sciences and Engineering under Award SCW0972-17. NTH work on vesicle fusion kinetics was supported by the Division of Materials Research of the National Science Foundation under an award 1710211. Drug delivery studies were supported by the LLNL

Laboratory Directed Research and Development (LDRD) Program under the award 18-ERD-011. Work at the Lawrence Livermore National Laboratory was performed under the auspices of the U.S. Department of Energy under Contract DE-AC52-07NA27344. Work at the Molecular Foundry was supported by the Office of Science, Office of Basic Energy Sciences, of the U.S. Department of Energy under Contract No. DE-AC02-05CH11231. MS, RMB, JK and GH work on computer simulations was supported by the Max Planck Society. MS and GH were supported by the Landes-Offensive zur Entwicklung Wissenschaftlich-ökonomischer Exzellenz (LOEWE) DynaMem program of the state of Hesse. JMH work on CNTP modifications and cell culture assays was supported by the Engineering and Physical Sciences Research Council [Grant number EP/R004072/1].

**Supplementary information.** Supplementary information available includes Materials and Methods, Supplementary Figures (S1-S18) and Table (S1), and Movies (S1, S2) showing fusion of vesicles stapled by CNTP monomers, dimers, and trimers in coarse-grained MD simulations.

Data availability. Experimental data presented in this work are available at <a href="https://figshare.com/s/64c2534665209a229a2e">https://figshare.com/s/64c2534665209a229a2e</a> (to be replaced by a permanent public DOI after manuscript acceptance), or from the corresponding authors upon request.

- 1. BG Katzung, Basic & Clinical Pharmacology. (McGraw-Hill, New York), 14th edition, (2018).
- BA Chabner, TG Roberts, Chemotherapy and the war on cancer. Nat. Rev. Cancer 5, 65–72 (2005).
- 3. BP Timko, et al., Advances in drug delivery. Annu. Rev. Mater. Res. 41, 1-20 (2011).
- L Sercombe, et al., Advances and challenges of liposome assisted drug delivery. Front. Pharmacol. 6, 286 (2015).
- Y Rosen, P Gurman, N Elman, Drug delivery: An integrated clinical and engineering approach. (CRC Press), (2017).
- D Peer, et al., Nanocarriers as an emerging platform for cancer therapy. Nat. Nanotechnol. 2, 751 (2007).
- C Zylberberg, S Matosevic, Pharmaceutical liposomal drug delivery: a review of new delivery systems and a look at the regulatory landscape. *Drug Deliv*. 23, 3319–3329 (2016).
- TM Allen, PR Cullis, Liposomal drug delivery systems: from concept to clinical applications. Adv. drug delivery reviews 65, 36–48 (2013).
- KB Knudsen, et al., In vivo toxicity of cationic micelles and liposomes. Nanomedicine 11, 467–477 (2015).
- MC Filion, NC Phillips, Major limitations in the use of cationic liposomes for DNA delivery. Int. J. Pharm. 162, 159–170 (1998).
- J Yang, et al., Drug delivery via cell membrane fusion using lipopeptide modified liposomes. ACS Cent. Sci. 2, 621–630 (2016).
- RM Bhaskara, SM Linker, M Vögele, J Köfinger, G Hummer, Carbon nanotubes mediate fusion of lipid vesicles. ACS Nano 11, 1273–1280 (2017).
- J Geng, et al., Stochastic transport through carbon nanotubes in lipid bilayers and live cell membranes. Nature 514, 612–615 (2014).
- 14. SC Harrison, Viral membrane fusion, Nat. Struct. & Mol. Biol. 15, 690 (2008)
- RM Epand, Fusion peptides and the mechanism of viral fusion. Biochimica et Biophys. Acta (BBA)-Biomembranes 1614, 116–121 (2003).
- L Earp, S Delos, H Park, J White, The many mechanisms of viral membrane fusion proteins in Membrane trafficking in viral replication. (Springer), pp. 25–66 (2004).
- M Kielian, FA Rey, Virus membrane-fusion proteins: More than one way to make a haripin. Nat. Rev. - Microbiol. 4, 67–76 (2005).
- DK Struck, D Hoekstra, RE Pagano, Use of resonance energy transfer to monitor membrane fusion. Biochemistry 20, 4093–4099 (1981).
- T Weber, et al., SNAREpins: minimal machinery for membrane fusion. Cell 92, 759–772 (1998).
- JM Hernandez, AJB Kreutzberger, V Kiessling, LK Tamm, R Jahn, Variable cooperativity in snare-mediated membrane fusion. *Proc. Natl. Acad. Sci.* 111, 12037–12042 (2014).
- C François-Martin, JE Rothman, F Pincet, Low energy cost for optimal speed and control of membrane fusion. *Proc. Natl. Acad. Sci. USA* 114, 1238–1241 (2017).
- F Fornasiero, et al., pH-tunable ion selectivity in carbon nanotube pores. Langmuir 26 14848–14853 (2010).
- R Tunuguntla, F Allen, K Kim, A Bellivieau, A Noy, Ultrafast proton transport in sub-1-nm diameter carbon nanotube porins. Nat. Nanotechnol. 11, 639–644 (2016).
- YC Barenholz, Doxil—the first FDA-approved nano-drug: lessons learned. J. Control. Release 160, 117–134 (2012).
- LM Russell, M Hultz, PC Searson, Leakage kinetics of the liposomal chemotherapeutic agent doxil: The role of dissolution, protonation, and passive transport, and implications for mechanism of action. J. Control. Release 269, 171–176 (2018).
- AL Seynhaeve, BM Dicheva, S Hoving, GA Koning, TL ten Hagen, Intact doxil is taken up intracellularly and released doxorubicin sequesters in the lysosome: evaluated by in vitro/in vivo live cell imaging. J. controlled release 172, 330–340 (2013).
- A Soundararajan, A Bao, WT Phillips, R Perez III, BA Goins, Re-liposomal doxorubicin (Doxil): In vitro stability, pharmacokinetics, imaging and biodistribution in a head and neck squamous cell carcinoma xenograft model. *Nucl. Medicine Biol.* 36, 515–524 (2009).
- T Tojima, Y Yamane, M Takahashi, E Ito, Acquisition of neuronal proteins during differentiation of NG108-15 cells. Neurosci. Res. 37, 153–161 (2000).

- 29. PS Kowalski, A Rudra, L Miao, DG Anderson, Delivering the messenger: advances in technologies for therapeutic mrna delivery. Mol. Ther. 27, 710 (2019).
- 30. A Ruggiero, et al., Paradoxical glomerular filtration of carbon nanotubes. *Proc. Natl. Acad.* Sci. USA 107, 12369–12374 (2010).
- TV Galassi, et al., Long-term in vivo biocompatibility of single walled carbon nanotubes. Plos
  One 15 (2020).
- 32. S Alidori, et al., Carbon nanotubes exhibit fibrillar pharmacology in primates. PloS One 12
  (2017).
- RH Tunuguntla, A Escalada, VA Frolov, A Noy, Synthesis, lipid membrane incorporation, and
  ion permeability testing of carbon nanotube porins. *Nat. Protoc.* 11, 2029 (2016).

586

587

588

589

- FJ Rawson, DJ Garrett, D Leech, AJ Downard, KH Baronian, Electron transfer from proteus vulgaris to a covalently assembled, single walled carbon nanotube electrode functionalised with osmium bipyridine complex: Application to a whole cell biosensor. *Biosens. Bioelectron.* 26, 2383–2389 (2011).
- 35. SG Ong, LC Ming, KS Lee, KH Yuen, Influence of the encapsulation efficiency and size of liposome on the oral bioavailability of griseofulvin-loaded liposomes. *Pharmaceutics* 8, 1–17
  (2016).
- 36. WW Focke, I Van der Westhuizen, N Musee, MT Loots, Kinetic interpretation of log-logistic
  dose-time response curves. Sci. Reports 7, 1–11 (2017).
- SJ Marrink, HJ Risselada, S Yefimov, DP Tieleman, AH De Vries, The MARTINI force field:
  Coarse grained model for biomolecular simulations. J. Phys. Chem. B 111, 7812–7824
  (2007).
- MJ Abraham, et al., GROMACS: High performance molecular simulations through multi-level
  parallelism from laptops to supercomputers. SoftwareX 1-2, 19–25 (2015).
- 39. DH De Jong, S Baoukina, HI Ingólfsson, SJ Marrink, Martini straight: Boosting performance
  using a shorter cutoff and GPUs. Comput. Phys. Commun. 199, 1–7 (2016).
- 40. G Bussi, D Donadio, M Parrinello, Canonical sampling through velocity rescaling. J. Chem.
  Phys. 126, 014101 (2007).
- 41. M Parrinello, A Rahman, Polymorphic transitions in single crystals: A new molecular dynamics method. J. Appl. Phys. 52, 7182–7190 (1981).
- 42. M Vögele, G Hummer, Divergent Diffusion Coefficients in Simulations of Fluids and Lipid
  Membranes. J. Phys. Chem. B 120, 8722–8732 (2016).

Ho, Siggel et al. PNAS | April 9, 2021 | vol. XXX | no. XX | 7